Research Square

Preprints are preliminary reports that have not undergone peer review.
They should not be considered conclusive, used to inform clinical practice,
or referenced by the media as validated information.

Residual-triggered active sensitivity estimation for topology-changes detection and voltage control with MAPO-SOP

Youzhuo Zheng
Guizhou Power Grid Co., Ltd
Yutao Xu
Guizhou Power Grid Co., Ltd
Yekui Yang
Guizhou Power Grid Co., Ltd
Yuchu Lu
Guizhou Power Grid Co., Ltd
Di Weng
Guizhou Power Grid Co., Ltd
Yanhong Jiang
1912986467@qq.com

Hunan University

Article

Keywords: distribution network reconfiguration, soft open point, model residual, active sensitivity estimation, voltage control

Posted Date: September 7th, 2026

DOI: https://doi.org/10.21203/rs.3.rs-10654574/v1

License: This work is licensed under a Creative Commons Attribution 4.0 International License.
Read Full License

Additional Declarations: No competing interests reported.

Version of Record: A version of this preprint was published at Scientific Reports on October 22nd, 2026. See the published version at https://doi.org/10.1038/s41598-026-76477-x.

Residual-triggered active sensitivity estimation for topology-changes detection and voltage control with MAPO-SOP

Youzhuo Zheng[a], Yutao Xu[a], Yekui Yang[a], Yuchu Lu[a], Di Weng[a], Yanhong Jiang*[b]

[a]Electric Power Research Institute, Guizhou Power Grid Co., Ltd., Guiyang 550002, China
[b]College of Electrical & Information Engineering, Hunan University, Changsha 410082, China

Corresponding author: Yanhong Jiang
Email:1912986467@qq.com
College of Electrical & Information Engineering, Hunan University, Changsha 410082, China

Abstract: Distribution-network reconfiguration changes the equivalent feeder impedance seen from a soft open point (SOP), thereby invalidating fixed-parameter analytical voltage-control models. This paper proposes a residual-triggered active sensitivity estimation method for model-assisted power optimization using an SOP (MAPO-SOP). An analytical point of common coupling (PCC) voltage model is first formulated to coordinate active and reactive power under the converter apparent-power constraint. Persistent voltage-prediction residuals are then used to identify potential model mismatch. Once triggered, a safety-oriented feedback controller returns the PCC voltage to a prescribed recovery band, after which a one-sided coordinated perturbation is applied to estimate the updated voltage–power sensitivity. The equivalent feeder parameters are subsequently reconstructed under the assumption that the X/R ratio remains approximately unchanged. In a 10-kV two-feeder system, the measured sensitivity-feature change indices were 33.58% and 57.44% for the two switching directions, with corresponding parameter errors of 2.8% and 0.2%. PV-only fluctuations did not trigger active estimation, whereas the combined PV/topology-change case was correctly identified with a parameter error of 0.42%. The proposed method enables temporary voltage containment and lightweight parameter adaptation without continuous probing or real-time topology communication.

Keywords: distribution network reconfiguration; soft open point; model residual; active sensitivity estimation; voltage control

1. Introduction

High penetrations of distributed photovoltaic (PV) generation increase operating uncertainty in distribution networks [1] [2]. At feeder-end buses, continuous changes in the local generation-load balance can lead to substantial voltage variations[3] [4].In distribution feeders, where resistance is non-negligible, voltage magnitude is influenced by both active and reactive power[5]. Conventional voltage regulation measures, including on-load tap changers, shunt compensators, inverter-based reactive power control, energy

storage, and active power curtailment, are constrained by discrete operation, limited converter capacity, investment cost, or curtailed energy. A soft open point (SOP), implemented using back-to-back power-electronic converters, provides continuous active-power exchange between adjacent feeders while independently regulating terminal reactive power [6] [7].

Existing SOP-based voltage control methods include centralized optimization, decentralized and local control, multistage coordination, and voltage stability enhancement [8] [9]. Although these methods improve power flow management and voltage regulation, their control laws generally require an accurate network topology, reliable line parameters, or valid voltage–power sensitivities. Switching operations that alter the supply path to a bus can therefore invalidate a fixed-parameter analytical controller. Sensitivity-based voltage controllers for changing network topologies have been investigated [10], but they do not directly address the recovery of a local analytical SOP controller following an abrupt model mismatch.

Distribution network topology and parameter identification has been investigated using model-based, statistical, and data driven methods [11], [12]. Smart meter and micro-phasor measurement unit data have been used for joint topology and parameter estimation [13-15]. These passive approaches can recover network structure without deliberate perturbations; however, their performance depends on measurement redundancy, observation-window length, natural excitation, and identifiability conditions [11] [12].

Active probing improves local identifiability by applying a controlled power perturbation and observing the resulting voltage response [16] [17]. Periodic probing, however, introduces unnecessary voltage deviations when the topology is unchanged, whereas purely passive estimation may remain uninformative when operating point variations are small [11] [12]. A practical SOP controller therefore requires a serial mechanism that first detects persistent model mismatch, temporarily contains the voltage deviation, and only then applies a short active perturbation to update the local-voltage power relation .

This paper develops a residual-triggered active sensitivity estimation method for model-assisted power optimization using a soft open point (MAPO-SOP). An analytical PCC-voltage model is established to derive a capacity-efficient active-reactive power coordination law for local voltage regulation. Model-prediction residuals are used to initiate a safety-oriented recovery process and event-triggered active probing, through which the post-reconfiguration voltage–power sensitivity is estimated. The equivalent feeder parameters are then reconstructed under an approximately invariant X/R ratio and embedded into the analytical controller. The proposed method is validated in a 10 kV two-feeder system under overvoltage, undervoltage, PV-fluctuation, and combined PV/topology-change conditions.

2. Methods

2.1 System configuration and PCC voltage model

Fig. 1 shows the flexibly interconnected two-feeder distribution system considered in this study. The two SOP converter ports share a common dc link. The two converter ports are connected through a common dc bus, and their control modes are listed in Table 1.

Table 1 Control Modes of SOP

No.	Control mode	Operating condition
1	PQ Control	Normal operation
2	$U_{dc}Q$ Control	Normal operation
3	Vf Control	Fault operation

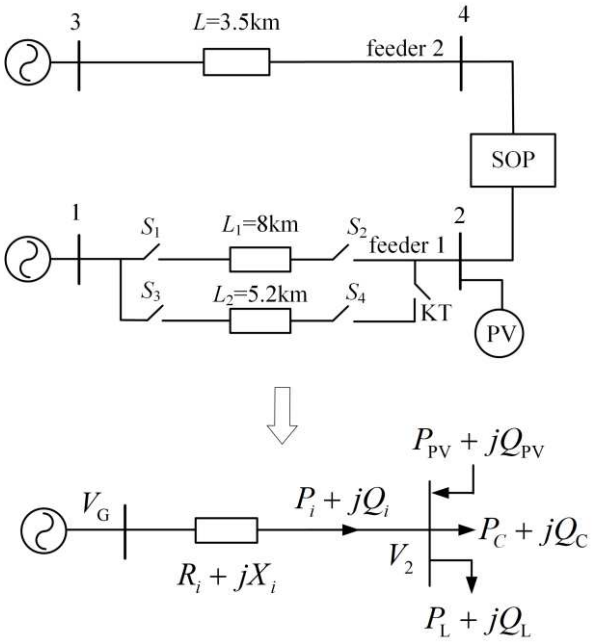


Fig. 1. Topology and equivalent circuit of the distribution network.

Under balanced three-phase operation and the small-angle approximation commonly adopted in branch-flow models, the quadrature component of the feeder voltage drop can be neglected. The rms line-to-line voltage at bus 2 is then approximated by [18] [19]

$$V_2 = \frac{V_G}{2} + \sqrt{\left(\frac{V_G}{2}\right)^2 + (P_{PV} - P_L)R - Q_L X - (P_C R + Q_C X)} \tag{1}$$

where V_G and V_2 denote the rms line-to-line voltages at the sending end of feeder 1 and at the PCC, respectively. P_{PV} is the PV active power output; P_L and Q_L are the active and reactive load powers; R and X are the equivalent resistance and reactance of feeder 1; and P_C and Q_C are the measured active and reactive powers transferred from bus 2 to the SOP.

Equation (1) separates the effects of the net generation–load balance, feeder impedance, and SOP power transfer on the PCC voltage. Under the adopted sign convention, increasing P_{PV} raises the PCC voltage, whereas positive P_C and Q_C reduce it. Because both R and X contribute to the feeder voltage drop, coordinated active-reactive power control can utilize the SOP converter capacity more effectively than reactive-power control alone [4] [5].

2.2 Optimal active-reactive power coordination

For fixed P_{PV}, P_L, Q_L, R and X, the voltage-regulation effect of the SOP is determined by $P_C R+Q_C X$. Maximizing its magnitude under the converter apparent-power constraint $P_C^2 + Q_C^2 \le S_C^2$ yields,

$$(P_C R + Q_C X)^2 \le (P_C^2 + Q_C^2)(R^2 + X^2) \le S_C^2 (R^2 + X^2) \tag{2}$$

where S_C is the apparent power limit of the bus 2 side converter. Equality holds when the SOP power vector is parallel to the feeder-impedance vector. The capacity-efficient coordination direction is therefore

$$Q_C = \lambda P_C, \quad \lambda = \frac{X}{R} \tag{3}$$

When reconfiguration replaces one supply path with another constructed from the same conductor family, R and X change approximately in the same proportion, and λ remains nearly constant. This assumption reduces the two-dimensional PQ allocation problem to a single control variable and is subsequently used to reconstruct the equivalent feeder parameters.

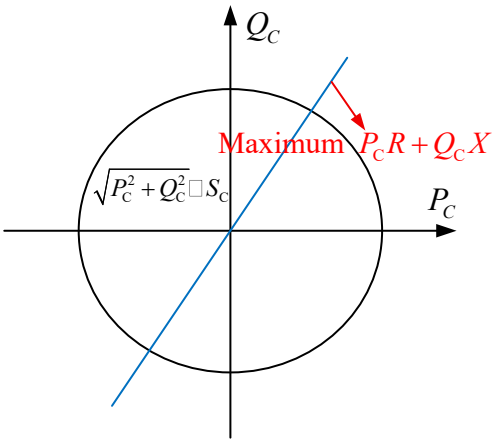


Fig. 2. SOP capacity circle and optimal active-reactive power coordination direction.

2.3 Continuous MAPO-SOP voltage regulation

MAPO-SOP first estimates the PCC voltage that would occur under the measured generation–load condition without additional SOP voltage-regulation action. It then calculates the active and reactive power required to move this inherent voltage to the applicable boundary of the target range. Let $\hat{R}$ and $\hat{X}$ denote the equivalent feeder parameters currently stored by the controller.

$$\hat{V}_{2,\text{in}}(t) = \frac{V_G(t)}{2} + \sqrt{\left(\frac{V_G(t)}{2}\right)^2 + \left[P_{PV}(t) - P_L(t)\right]\hat{R} - Q_L(t)\hat{X}} \tag{4}$$

$$V_{2,\text{tar}}(t) = \begin{cases} 10.3\text{kV}, & \hat{V}_{2,\text{in}}(t) > 10.3\text{kV} \\ 9.7\text{kV}, & \hat{V}_{2,\text{in}}(t) < 9.7\text{kV} \\ \hat{V}_{2,\text{in}}, & 9.7 \le \hat{V}_{2,\text{in}}(t) \le 10.3\text{kV} \end{cases} \tag{5}$$

where $\hat{V}_{2,\text{in}}$ is the inherent PCC voltage estimate calculated from the current measurements and the stored line parameters $\hat{R}$ and $\hat{X}$; $V_{2,\text{tar}}$ is the selected PCC target voltage. The normal PCC-voltage target band is 9.70-10.30 kV. When $\hat{V}_{2,\text{in}}$ exceeds the upper boundary, 10.30 kV is selected as the target voltage; when it falls below the lower boundary, 9.70 kV is selected. If the inherent voltage remains within the band, no additional voltage-regulation command is generated.

Combining (1), (3), and the selected target voltage yields the analytical SOP power references in (6),

$$\begin{bmatrix} P_{C,\text{ref}}(t) \\ Q_{C,\text{ref}}(t) \end{bmatrix} = \frac{1}{\hat{R}^2 + \hat{X}^2} \begin{bmatrix} \hat{R} \\ \hat{X} \end{bmatrix} \left[\left(\hat{V}_{2,\text{in}} - \frac{V_G}{2}\right)^2 - \left(V_{2,\text{tar}} - \frac{V_G}{2}\right)^2 \right] \tag{6}$$

where $P_{C,ref}$ and $Q_{C,ref}$ are the active and reactive power commands. When the inherent voltage exceeds the target, both references are positive and the SOP absorbs power from bus 2, thereby reducing the PCC voltage. The opposite power direction is obtained under undervoltage conditions.

When $\hat{R}=R$ and $\hat{X}=X$, (4)-(6) provide the corrective power predicted by the analytical voltage model. After feeder reconfiguration, however, the actual supply-path parameters may change while the controller continues to use their pre-change values. The resulting mismatch affects both the inherent-voltage estimate and the calculated SOP power, motivating online residual monitoring and parameter adaptation.

2.4 One-dimensional sensitivity and equivalent impedance feature

Equation (1) defines the PCC voltage as a function of the two SOP power components. Differentiation with respect to PC and QC gives the local sensitivities K_{uP} and K_{uQ} in (7).

$$K_{uP}=\frac{\partial V_2}{\partial P_C}=-\frac{R}{2\left(V_2-\frac{V_G}{2}\right)},\quad K_{uQ}=\frac{\partial V_2}{\partial Q_C}=-\frac{X}{2\left(V_2-\frac{V_G}{2}\right)} \tag{7}$$

Rather than applying independent active- and reactive-power perturbations, the proposed estimator varies the SOP power along $Q_C=\lambda P_C$. The resulting voltage-to-active-power sensitivity along the coordinated direction is given by (8).

$$K_u=\frac{\mathrm{d}V_2}{\mathrm{d}P_C}=K_{uP}+\lambda K_{uQ}=-\frac{R^2+X^2}{2R\left(V_2-\frac{V_G}{2}\right)} \tag{8}$$

The sensitivity K_u is estimated from two adjacent quasi-steady-state operating points [17]. Operating point 0 is recorded before the perturbation, whereas operating point 1 is recorded after the converter response has settled. To reduce the influence of reference-tracking error, the denominator in (9) uses the measured change in actual SOP active power rather than the commanded perturbation. An overbar denotes the average value over the corresponding steady-state measurement window.

$$K_u=\frac{\bar{V}_{2,1}-\bar{V}_{2,0}}{\bar{P}_{C,1}-\bar{P}_{C,0}},\quad \bar{Q}_{C,1}-\bar{Q}_{C,0}\approx\lambda\left(\bar{P}_{C,1}-\bar{P}_{C,0}\right) \tag{9}$$

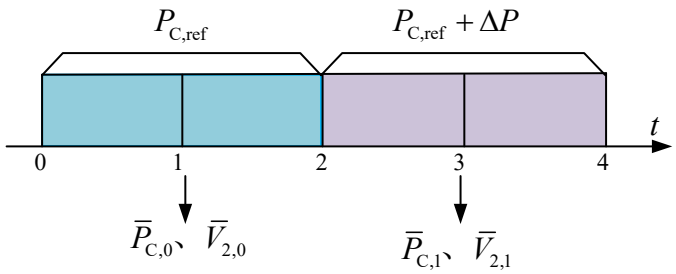


Fig. 3. Timing diagram for finite difference sensitivity estimation.

To remove the influence of the operating voltage on the magnitude of K_u, the equivalent sensitivity feature along the optimal coordination direction is defined as

$$\Gamma_u=-2\left(V_2-\frac{V_G}{2}\right)K_u=R+\lambda_0 X \tag{10}$$

Normalizing K_u by the local operating voltage gives the equivalent sensitivity feature $\Gamma_u=R+\lambda_0 X$. When X/R remains close to λ_0, Γ_u is approximately independent of the PCC operating voltage and changes mainly with the active supply path impedance.

2.5 Fixed parameter model mismatch after a topology change

Before reconfiguration, the actual feeder parameters and the parameters stored by the controller are R_0 and X_0. After a sectionalizing or tie switch, the actual parameters change to R_1 and X_1, while the controller temporarily retains R_0 and X_0. Consequently, the predicted PCC voltage deviates from the measured voltage.

$$r_V(t)=V_2(t)-V_{2,\mathrm{pred}}(t) \tag{11}$$

where $V_{2,\mathrm{pred}}$ is the voltage predicted by substituting R_0 and X_0, the measured generation and load powers, and the actual SOP powers into (1). Letting $\Delta R=R_1-R_0$ and $\Delta X=X_1-X_0$, a first-order linearization of (1) around the pre-change operating point gives the topology-induced voltage deviation in (12).

$$r_V \approx \frac{(P_{PV}-P_L-P_C)\Delta R-(Q_L+Q_C)\Delta X}{2\left(V_{2,\mathrm{pred}}-\dfrac{V_G}{2}\right)} \tag{12}$$

The residual is not unique to a topology change. Measurement errors, time misalignment among measured quantities, variations in the sending-end voltage, and incomplete SOP power tracking can also produce transient residuals. The residual is therefore used only as a preliminary indicator of model mismatch, rather than as direct evidence of a topology change.

2.6. Residual-triggered topology change detection and parameter adaptation

The proposed procedure consists of four sequential stages: residual-based mismatch detection, safety-oriented voltage recovery, active sensitivity estimation, and equivalent-parameter reconstruction, as summarized in Fig. 4. Residual monitoring avoids unnecessary probing during normal operation, while the recovery loop prevents the PCC voltage from deteriorating after the analytical model has been declared invalid.

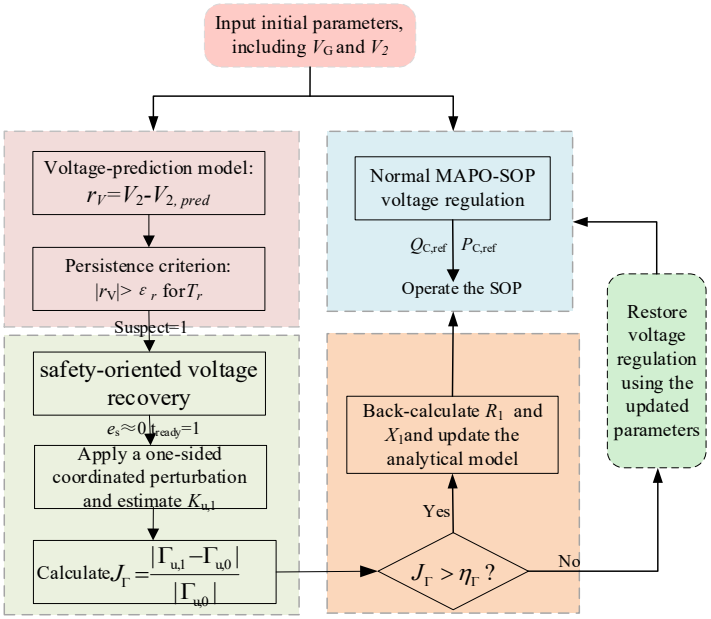


Fig. 4. Residual-triggered safety recovery, active sensitivity estimation, and equivalent-parameter update procedure.

2.6.1 Residual detection and safety-oriented voltage recovery

When the stored parameters match the actual feeder parameters, the analytical model is consistent with the physical system and V_2 remains close to $V_{2,\mathrm{pred}}$ at steady state. A topology change introduces a persistent residual through the parameter increments in (12). A suspected model mismatch is declared only when the residual magnitude remains above ε_r for the specified persistence time T_r.

$$\mathrm{Suspect}=\begin{cases}1, & |r_V(\tau)|>\varepsilon_r,\quad \forall\tau\in[t-T_r,t]\\ 0, & \text{otherwise.}\end{cases} \tag{13}$$

where ε_r is the residual threshold, T_r is the persistence time, and Suspect is a latched model-mismatch flag.

When Suspect changes from 0 to 1, the analytical MAPO-SOP command is disabled and the safety-oriented recovery loop is activated. The signed voltage error e_s is defined relative to the inner recovery band $[V_{\mathrm{low}}, V_{\mathrm{high}}]$, where V_{low}=9.85 kV and V_{high}=10.15 kV.

$$e_s=\begin{cases}V_2-V_{\mathrm{high}}, & V_2>V_{\mathrm{high}},\\ 0, & V_{\mathrm{low}}\le V_2\le V_{\mathrm{high}}\\ V_2-V_{\mathrm{low}}, & V_2<V_{\mathrm{low}},\end{cases} \tag{14}$$

Because the stored $\hat{R}$ and $\hat{X}$ values may no longer be valid, the recovery loop does not use them to calculate the corrective power magnitude. Instead, it retains the sign and a bounded conservative magnitude of the most recently accepted sensitivity. The safe sensitivity is defined as

$$K_{\mathrm{safe}}=-\mathrm{clip}\left(|\hat{K}_{u,0}|,0.80,1.00\right) \tag{15}$$

where clip (x, a, b) restricts x to the interval [a, b].

The safety-oriented active-power command is updated at each control instant according to (16), and the reactive-power command follows the coordinated direction $Q_{\mathrm{safe}}=\lambda_0 P_{\mathrm{safe}}$. The coordinated command is projected onto the 1.90-MVA converter-capacity boundary.

$$P_{\mathrm{safe}}[k]=\mathrm{sat}\left\{P_{\mathrm{safe}}[k-1]-\gamma_{\mathrm{safe}}\frac{e_s[k]}{K_{\mathrm{safe}}}\right\},\quad Q_{\mathrm{safe}}[k]=\lambda_0 P_{\mathrm{safe}}[k] \tag{16}$$

The update gain is γ_{safe} =0.5 and the control interval is 0.02 s. Active estimation is enabled when the PCC voltage remains within 0.02 kV of either recovery boundary for 0.06 s. Only one readiness pulse is issued during each Suspect event. Estimation is inhibited whenever the PCC voltage leaves the 9.5–10.5 kV permission range.

2.6.2 Active sensitivity estimation under a coordinated perturbation

Active sensitivity estimation begins only after the recovery and power-tracking conditions have been satisfied. The current safe operating point is then latched as the perturbation centre, and a one-sided active-power increment is applied along the coordinated direction in (17).

$$\begin{bmatrix}P_{C,1}^{\mathrm{ref}}\\ Q_{C,1}^{\mathrm{ref}}\end{bmatrix}=\begin{bmatrix}P_{C,0}^{\mathrm{ref}}\\ Q_{C,0}^{\mathrm{ref}}\end{bmatrix}+s_{\mathrm{id}}\Delta P_{\mathrm{id}}\begin{bmatrix}1\\ \lambda_0\end{bmatrix} \tag{17}$$

In (17), subscripts 0 and 1 denote the reference operating points before and after the perturbation, respectively; $\Delta P_{\mathrm{id}}>0$ is the active-power perturbation magnitude; and s_{id} is selected as +1 for the overvoltage case and -1 for the undervoltage case. The two averaged operating points are subsequently used in (9). An

estimation result is accepted only if the measured active-power change exceeds a prescribed minimum value and the averaged *PQ* increment remains sufficiently aligned with the coordination direction.

2.6.3 Topology change decision and parameter reconstruction

The relative change in the equivalent sensitivity feature is evaluated using (18),

$$J_\Gamma = \left| \frac{\hat{\Gamma}_{\mathrm{u},1} - \hat{\Gamma}_{\mathrm{u},0}}{\hat{\Gamma}_{\mathrm{u},0}} \right|, \quad J_\Gamma > \eta_\Gamma \tag{18}$$

where $\hat{\Gamma}_{u0}$ is the currently accepted baseline feature and $\hat{\Gamma}_{u1}$ is obtained from the new perturbation. A value $J_\Gamma > \eta_\Gamma$ confirms a significant change in the equivalent supply-path impedance; otherwise, the stored line parameters are retained.

If the post-change path also satisfies $X_1/R_1 \approx \lambda_0$, the equivalent feeder parameters are reconstructed from the measured sensitivity feature using (19). After a successful update, $\hat{\Gamma}_{u1}$ becomes the new baseline, and the MAPO-SOP analytical controller resumes operation using the reconstructed parameters.

$$\hat{R}_1 = \frac{\hat{\Gamma}_{\mathrm{u}}}{1+\lambda_0^2} = -\frac{2\left(V_{2,\mathrm{id}} - \dfrac{V_{G,\mathrm{id}}}{2}\right)\hat{K}_{\mathrm{u}}}{1+\lambda_0^2}, \quad \hat{X}_1 = \lambda_0 \hat{R}_1 \tag{19}$$

where $\hat{R}_1$ and $\hat{X}_1$ are the reconstructed equivalent line parameters.

3. Results

3.1 Test system and simulation settings

The proposed method is evaluated using a 10 kV flexibly interconnected two-feeder system. The bus-2-side converter operated in PQ control, whereas the bus-4-side converter regulated the common dc-link voltage. Feeder 1 is supplied through either the 8.0 km path L_1 or the 5.2 km path L_2. The normal PCC-voltage target band is 9.70–10.30 kV, the inner recovery band is 9.85–10.15 kV, and the safety-oriented apparent-power command is limited to 1.90 MVA. The principal network, control, and detection parameters are summarized in Tables 1 and 2.

Table 2. Main simulation and control parameters.

Parameter	Value	Parameter	Value
Resistance per unit length, r_0	0.21 Ω/km	Long backup supply path, L_1	8.0 km
Reactance per unit length, x_0	0.373 Ω/km	Short tie supply path, L_2	5.2 km
PV capacity at bus 2	2 MVA	Model residual threshold, ε_r	0.06 kV
Active load range at bus 2	1.1~4.2 MW	Residual persistence time, T_r	0.10 s
Reactive load range at bus 2	0.362~ 1.38 Mvar	Equivalent sensitivity change threshold, η_Γ	0.30

3.2 Topology change cases

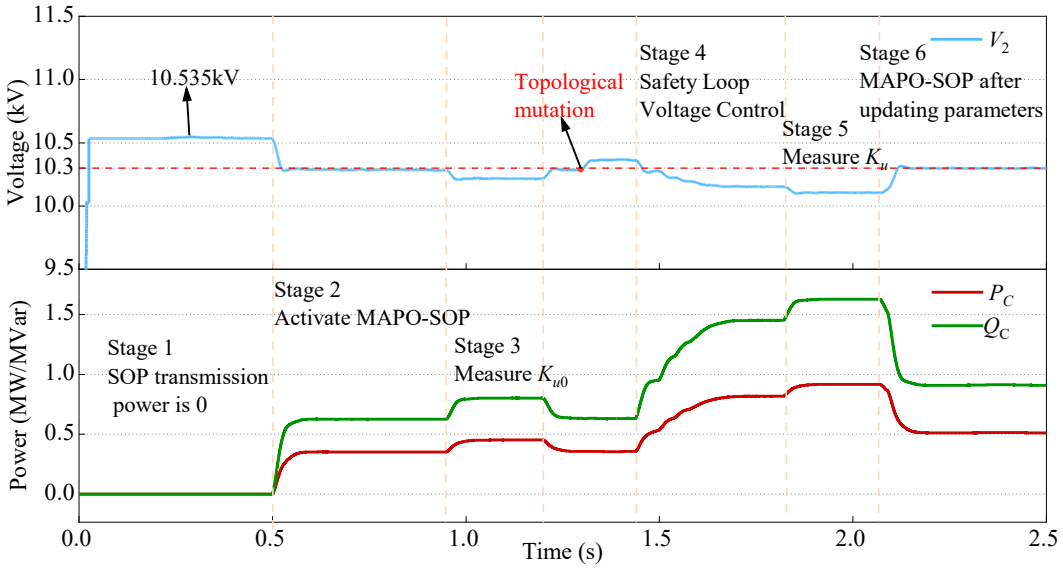
The bidirectional regulation capability is evaluated under a high-PV/light-load condition and a zero-PV/heavy-load condition. In both cases, the bus-4-side converter is enabled at 0.10 s, the bus-2-side converter at 0.20 s, MAPO-SOP regulation at 0.50 s, and the initial sensitivity measurement at 0.80 s. The supply-path switching event is applied at 1.30 s.

3.2.1 Overvoltage Case

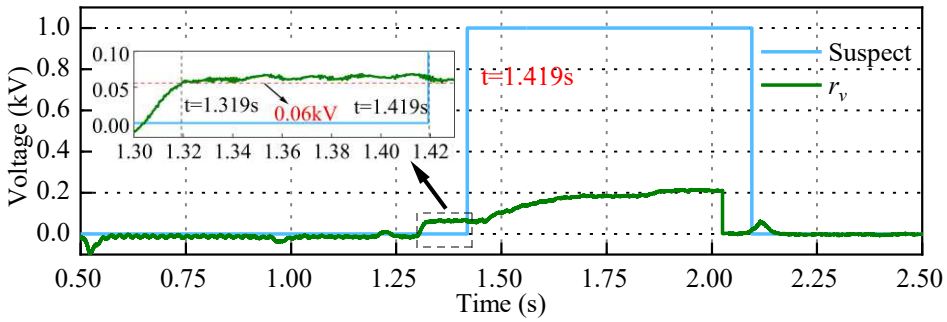
As shown in Fig. 5 ,the initial path is L_1, the PV output is 2.0 MW, and the bus-2-load is 1.10 MW+j0.362 MVar. Without SOP regulation, the PCC voltage is approximately 10.535 kV. After MAPO-SOP regulation is enabled at 0.50 s, the SOP transferred 0.354 MW and 0.630 MVAr, maintaining the PCC voltage near 10.288 kV. The initial equivalent sensitivity feature is estimated as 7.022 Ω.

At 1.30 s, the supply path is switched from L_1 to L_2, while the controller continued to use the parameters. The PCC voltage consequently increased to 10.365 kV. The residual exceeded 0.06 kV at 1.319 s, and Suspect is asserted at 1.419 s. The safety-oriented loop then reduced the voltage to 10.152 kV by 1.675 s, after which active sensitivity estimation is initiated. The post-change feature is estimated as 4.664 Ω at 2.025 s.

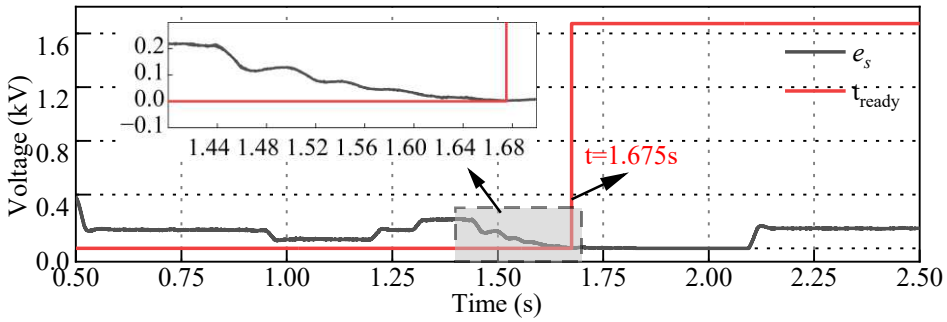
The theoretical equivalent feature decreases from 6.980 to 4.537 Ω for the L_1-to-L_2 transition, corresponding to a 35.0% reduction. The measured change index is 33.58%, exceeding the 30% confirmation threshold. The reconstructed parameters are $\hat{R}$=1.123 Ω and $\hat{X}$=1.994 Ω, each with an error of 2.8%. After the updated parameters are applied, the PCC voltage settled at 10.297 kV. The SOP command remained within the 1.90 MVA safety-control limit throughout the recovery and estimation stages.



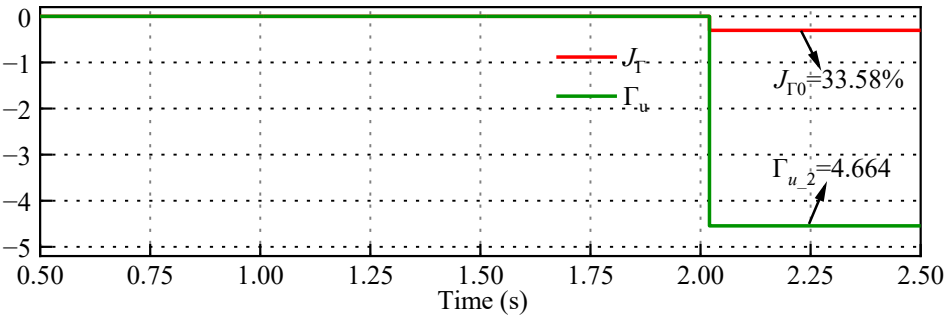
(a) PCC voltage and SOP port powers



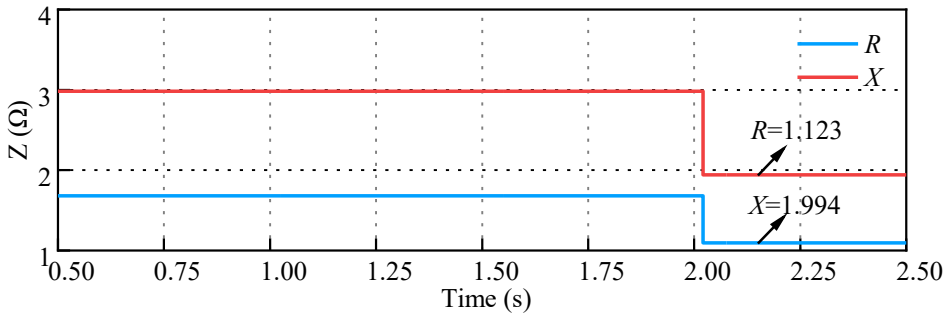
(b) Residual trigger signal



(c) Safety recovery signal



(d) Equivalent sensitivity feature



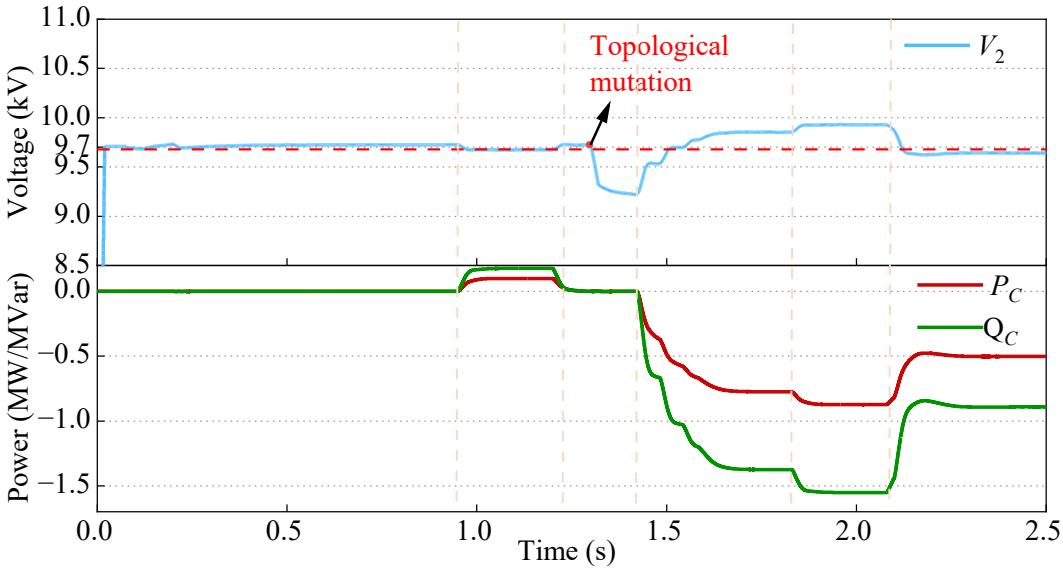
(e) Equivalent resistance and reactance

Fig. 5. Overvoltage case under high PV/light load operation.

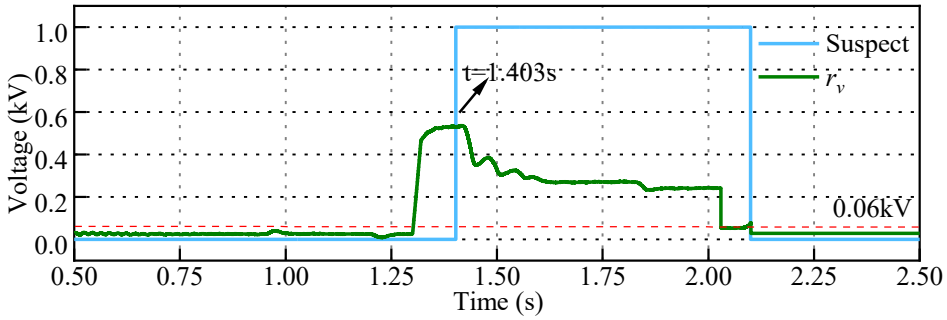
3.2.2 Undervoltage Case

The initial path was L_2, the PV output was zero, and the bus 2 load was 4.20 MW + j1.380 MVar. Switching from L_2 to L_1 at 1.30 s caused the PCC voltage to decrease to approximately 9.223 kV because the controller retained the L_2 parameters. Suspect was asserted at approximately 1.403 s, and the safety-oriented loop restored the voltage to the 9.85-kV recovery boundary by approximately 1.680 s. The equivalent sensitivity features measured before and after switching are 4.442 and 6.993 Ω, respectively.

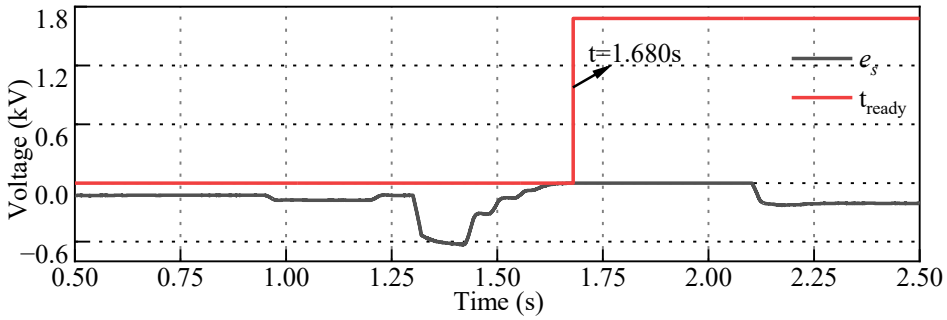
The theoretical equivalent feature increases from 4.537 to 6.980 Ω, corresponding to a 53.84% change. The measured change index was 57.44%, exceeding the topology-confirmation threshold. The reconstructed values were $\hat{R}$ = 1.683 Ω and $\hat{X}$ = 2.990 Ω, with a 0.2% relative error. After parameter updating, the SOP powers settled at -0.502 MW and -0.891 MVar and the PCC voltage settled at 9.663 kV.



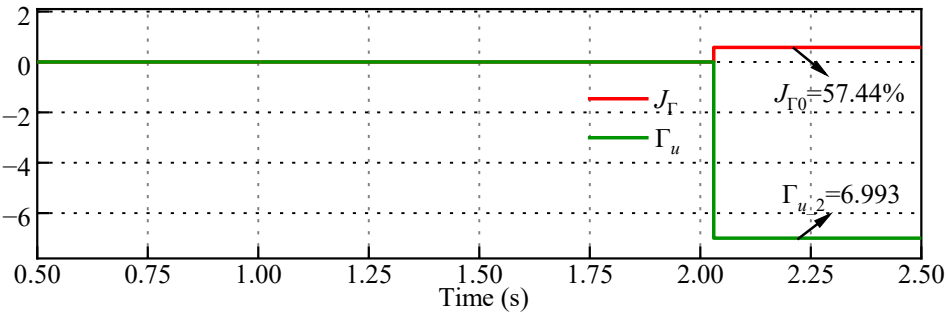
(a) PCC voltage and SOP port powers



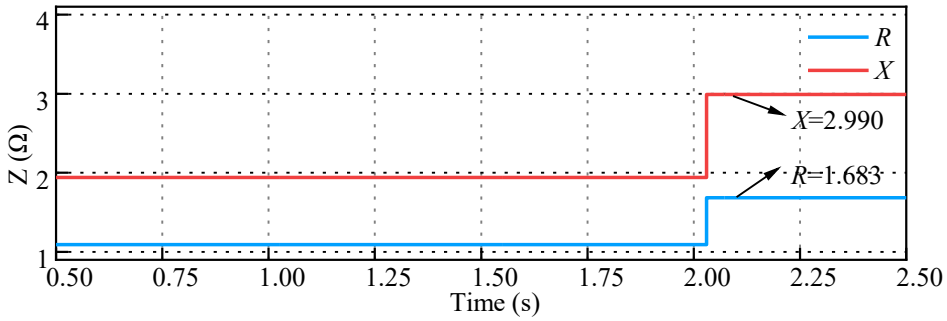
(b) Residual trigger signal



(c) Safety recovery signal



(d) Equivalent sensitivity feature



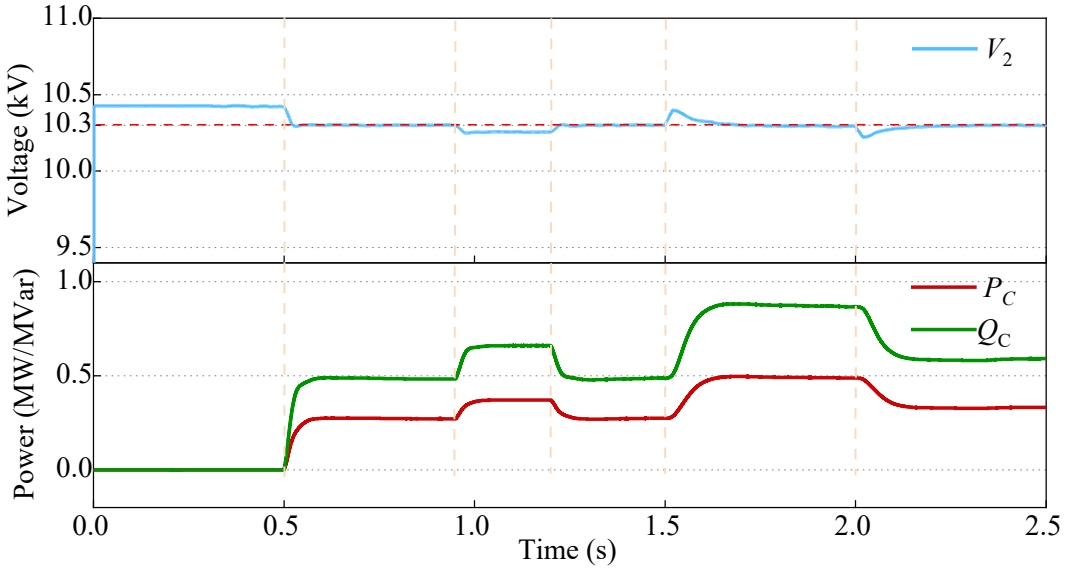
(e) Equivalent resistance and reactance

Fig. 6. Undervoltage case under zero PV/heavy load operation.

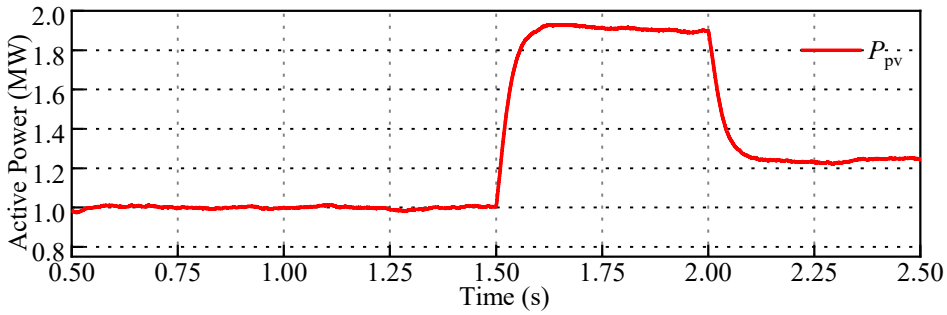
3.3 Detection reliability under PV fluctuations

3.3.1 PV fluctuations with unchanged topology

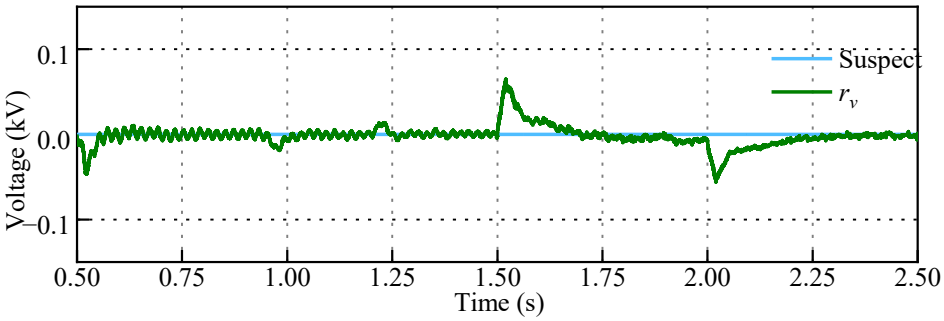
To evaluate resistance to false triggering, the topology is fixed at L_1 and the bus2 load is maintained at 1.10 MW + j0.362 MVar. The PV active-power output increased from 1.0 to 2.0 MW during 1.50-2.00 s and then decreased to 1.25 MW. Because the feeder parameters remained unchanged, no active sensitivity estimation is expected.



(a) PCC voltage and SOP port powers



(b) Photovoltaic active power output



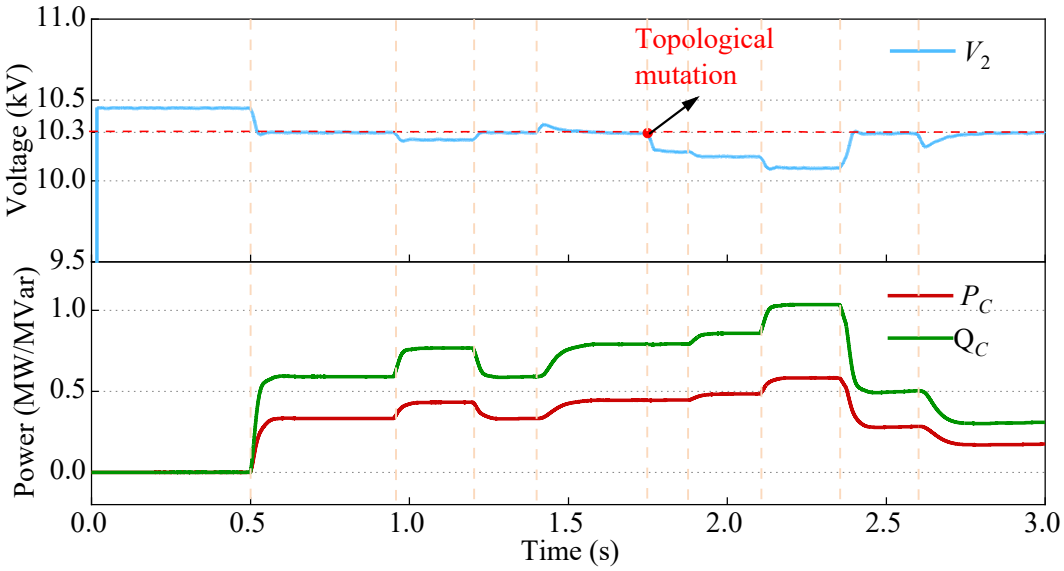
(c) Residual trigger signal

Fig. 7. PV fluctuation case with unchanged topology.

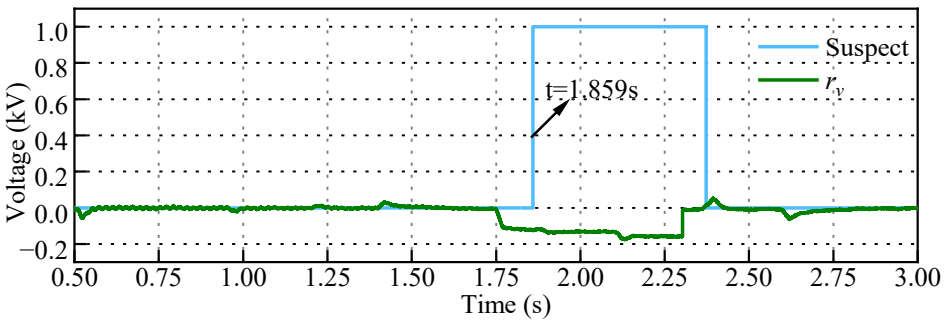
MAPO-SOP adjusted the SOP active and reactive powers in response to the PV variation and maintained the PCC voltage close to the 10.30 kV upper target boundary. The residual peaks at the beginning of the upward and downward PV ramps were 0.061 and 0.054 kV, respectively. In both cases, the residual remained above 0.06 kV for less than the 0.10 s persistence time; consequently, neither Suspect nor active sensitivity estimation is triggered. The result confirms that the persistence criterion rejects short residual excursions caused by ordinary generation load transients.

3.3.2 Combined PV fluctuation and topology switching

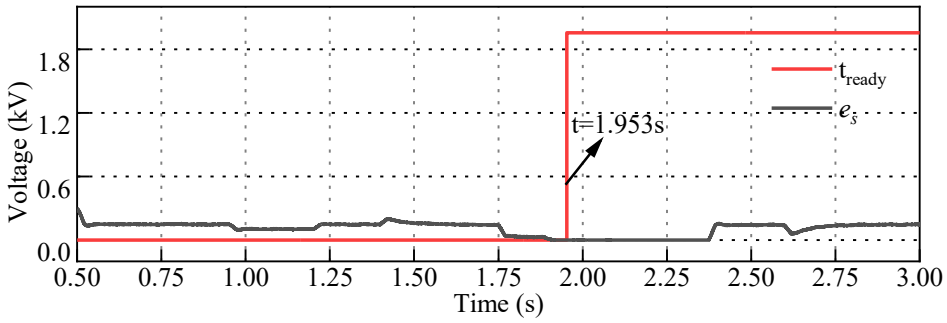
The combined-disturbance test used L_2 as the initial supply path and a load of 1.10 MW + j0.362 MVar. The PV output increased from 1.25 to 1.60 MW during 1.40-2.60 s and then decreased to 1.25 MW. The supply path is switched from L_2 to L_1 at 1.75 s while the PV output is still varying.



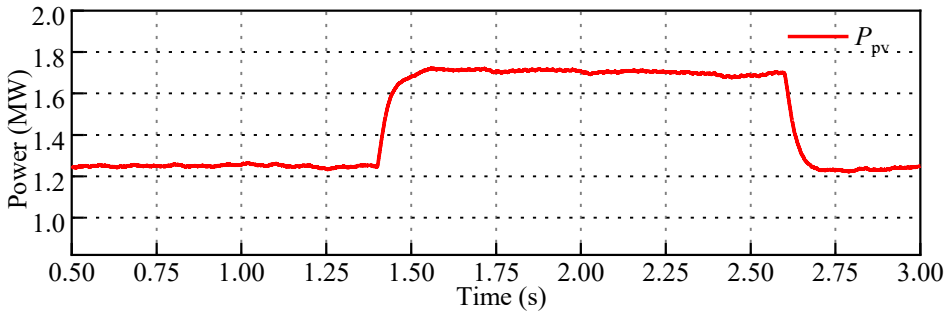
(a) PCC voltage and SOP port powers



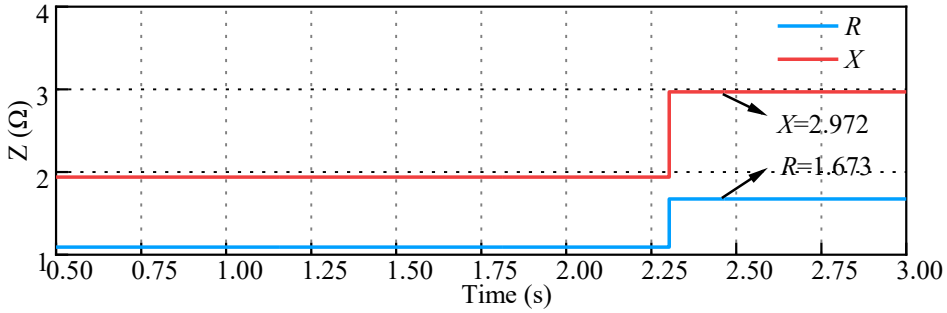
(b) Residual trigger signal



(c) Safety recovery signal



(d) Photovoltaic active power output



(e) Equivalent resistance and reactance

Fig. 8. Combined PV fluctuation and topology switching case.

The PV ramp alone did not satisfy the residual-persistence criterion. Following the topology change at 1.75 s, Suspect is asserted at 1.859 s and the readiness condition for active estimation is satisfied at 1.953 s. The theoretical equivalent feature increases from 4.537 to 6.980 Ω for the L_2 to L_1 transition. The measured values were 4.482 and 6.964 Ω, giving a 55.38% change index, which exceeded the 30% threshold. The reconstructed parameters were $\hat{R} = 1.673$ Ω and $\hat{X} = 2.972$ Ω, with a reported relative error of 0.42%. The PCC voltage finally settled at 10.298 kV.

4. Conclusions

This paper proposes a residual-triggered active sensitivity estimation method for MAPO-SOP voltage control under supply-path changes. Persistent voltage-prediction residuals are used to identify potential model mismatch, after which a safety-oriented feedback loop temporarily contains the PCC-voltage deviation. Active sensitivity estimation is initiated only after the voltage and power-tracking conditions have been satisfied, and the equivalent feeder parameters are reconstructed under an approximately constant X/R ratio.

In the two topology-switching cases, the measured equivalent-feature change indices are 33.58% and 57.44%, and the corresponding parameter-reconstruction errors are 2.8% and 0.2%, respectively. PV-only fluctuations do not satisfy the residual-persistence criterion and therefore do not trigger active estimation. Under combined PV fluctuations and topology switching, the method yields a feature-change index of 55.38%

and a parameter error of 0.42%. The method provides temporary voltage containment and local parameter adaptation without continuous probing or real-time topology communication.

Data availability

The datasets generated during and/or analysed during the current study are not publicly available due to confidentiality concerns but are available from the corresponding author on reasonable request.

Acknowledgements

This research was supported by Electric Power Research Institute, Guizhou Power Grid Co., Ltd. Technology Project (GZKJXM20232428)

Author contributions

Youzhuo Zheng: Conceptualization (equal). Yutao Xu: Supervision (equal)**.** Yekui Yang: Resources (equal). Yuchu Lu: Validation (equal). Di Weng: Data curation (equal), Writing – original draft (equal). Yanhong Jiang: Writing – review & editing (equal).

Competing interests

The authors declare no competing interests.

References

[1] Zhang, S., Yang, G., He, J. et al. Research on optimal dispatching and protection methods for high-proportion renewable energy distribution networks. Power Big Data 28, 1-9 (2025).

[2] Sun, X., Zeng, J., Liu, J. et al. An optimal allocation method for distributed photovoltaic considering output uncertainty. Hunan Electric Power 44, 10-16 (2024).

[3] Diahovchenko, I., Morva, G., Chuprun, A. and Keane, A. Comparison of voltage rise mitigation strategies for distribution networks with high photovoltaic penetration. Renew. Sustain. Energy Rev. 212, 115399 (2025).

[4] Hu, R., Wang, W., Wu, X. et al. Coordinated active and reactive power control for distribution networks with high penetrations of photovoltaic systems. Sol. Energy 231, 809-827 (2022).

[5] Hu, X., Liu, Z.-W., Wen, G., Yu, X. and Liu, C. Voltage control for distribution networks via coordinated regulation of active and reactive power of DGs. IEEE Trans. Smart Grid 11, 4017-4031 (2020).

[6] Cao, W., Wu, J., Jenkins, N., Wang, C. and Green, T. C. Operating principle of Soft Open Points for electrical distribution network operation. Appl. Energy 164, 245-257 (2016).

[7] Cao, W., Wu, J., Jenkins, N., Wang, C. and Green, T. C. Benefits analysis of Soft Open Points for electrical distribution network operation. Appl. Energy 165, 36-47 (2016).

[8] Li, P., Ji, H., Yu, H. et al. Combined decentralized and local voltage control strategy of soft open points in active distribution networks. Appl. Energy 241, 613-624 (2019).

[9] Pamshetti, V. B., Singh, S., Thakur, A. K. et al. Multistage coordination Volt/VAR control with CVR in active distribution network in presence of inverter-based DG units and soft open points. IEEE Trans. Ind. Appl. 57, 2035-2047 (2021).

[10] Xiong, W., Tang, Z. and Cui, X. Distributed data-driven voltage control for active distribution networks with changing grid topologies. Control Eng. Pract. 147, 105933 (2024).

[11] Dalavi, F., Hamedani Golshan, M. E. and Hatziargyriou, N. D. A review on topology identification methods and applications in distribution networks. Electr. Power Syst. Res. 234, 110538 (2024).
[12] Deka, D., Kekatos, V. and Cavraro, G. Learning distribution grid topologies: A tutorial. IEEE Trans. Smart Grid 15, 999-1013 (2024).
[13] Srinivas, V. L. and Wu, J. Topology and parameter identification of distribution network using smart meter and μPMU measurements. IEEE Trans. Instrum. Meas. 71, 9004114 (2022).
[14] Guo, Y., Yuan, Y. and Wang, Z. Distribution grid modeling using smart meter data. IEEE Trans. Power Syst. 37, 1995-2004 (2022).
[15] Zhang, J., Wang, Y., Weng, Y. and Zhang, N. Topology identification and line parameter estimation for non-PMU distribution network: A numerical method. IEEE Trans. Smart Grid 11, 4440-4453 (2020).
[16] Cavraro, G. and Kekatos, V. Inverter probing for power distribution network topology processing. IEEE Trans. Control Netw. Syst. 6, 980-992 (2019).
[17] Huang, C., Burroughs, H., Klauber, C. and Sun, C.-C. Power distribution system characterization with active probing: Real-world testing and analysis. IEEE Open Access J. Power Energy 10, 86-92 (2023).
[18] Baran, M. E. and Wu, F. F. Optimal sizing of capacitors placed on a radial distribution system. IEEE Trans. Power Deliv. 4, 735-743 (1989).
[19] Farivar, M. and Low, S. H. Branch flow model: Relaxations and convexification-Part I. IEEE Trans. Power Syst. 28, 2554-2564 (2013).
[20]